Design of a Compact Hybrid Moore's Fractal Inspired Wearable Antenna for IOT Enabled Bio-telemetry in Diagnostic Health Monitoring System

Mrs.K.MEERA, ME (VLSI DESIGN)
DEPARTMENT OF ECE
VANDAYAR ENGINEERING COLLEGE,

Mrs.J.JANANI , B.E,M.TECH.,
ASSISTANT PROFESSOR,
DEPARTMENT OF ECE
VANDAYAR ENGINEERING COLLEGE

ABSTRACT Since the Internet of Things (IoT) enabled medical diagnostic system requires unprecedented precision and automation for better health care delivery, therefore in such systems, the performance of antennas for efficiently transferring data (vital functions of the human body) is an important task. To address these concerns, a mechanically robust, novel hybrid wearable on-body antenna inspired by Moore's fractal-based geometry and conventional rectangular loop for a diagnostic health monitoring system is proposed. The structure developed involves the etching of Moore's curve onto a conventional rectangular patch and subsequently encasing it in a rectangular loop along with a defected ground structure. The proposed antennaexhibits dual-band with bandwidth ranging from 1.38 - 1.8 GHz and 2.25 - 4.88 GHz respectively, covering WMTS, ISM, and Personal Communication band besides covering a portion of UWB band also. The two operating bands of the antenna offer a fractional bandwidth of 38.5% and 73.7% respectively. It is observed that the average specific absorption rate (SAR) over the multi-layer phantom is 0.025 W/kg for an input power of 24 dBm. In comparison to the recently reported wearable antennas, the design proposed has a compact footprint of 0.135 λo x 0.093λo x 0.004λo besides offering a dual- band of operation, peak gainof 2.2 dBi, overall radiated efficiency of 95% and SAR below 0.025 W/kg. The design is fabricated using Rogers 5880 substrate (semi-flex) of thickness 0.75 mm. The experimental results validate the simulated results making the proposed antenna a promising candidate for the bio-medical application. On analysing the performance of the proposed antenna onto the human body (human body loading), it is concluded that the proposed antenna structure is appropriate for bio-telemetric application in diagnostic health monitoring systems wherein data is relayed from all bio-sensors to remote control systems.

INDEX TERMS Bio-sensor, Internet of Things (IoT), personal communication band, specific absorption, rate (SAR), ultra-wideband (UWB), wireless medical telemetry services (WMTS).

I. INTRODUCTION

From the last two years, our society at large is facing the disastrous outcomes of the pandemic. It is an undeniable fact that the healthcare sector is the worst hit and there has been tremendous pressure on its resources. People working in the biomedical field are not only trying to fix the challenge arising due to the unexpected situation but also aim to provide a steady solution for the future whenever such a critical situation arises. In light of this situation, a lot of work has

The associate editor coordinating the review of this manuscript and approving it for publication was Masood Ur-Rehman .

been done to decrease the workload of doctors by reducing the number of visits of patients to the hospitals. This has been achieved by ensuring proper telemonitoring of vital functions of critical patients and a timely diagnosis by the healthcare professionals.

In a biomedical diagnostic system, an antenna is not only a vital part of the system but it defines the overall efficacy of the system [1]. A schematic of the biotelemetry-based diagnostic health monitoring system is illustrated in Fig. 1. Designing an antenna for on-body application is a herculean task. In such scenarios, the RF waves interact with different tissues of the body resulting in internal reflection and scattering phenomena which makes the impedance matching a hectic issue. Not only this, the placement of the antenna once fixed over a human body is liable to change whenever any body movement occurs. This results in a change in the resonant frequency, impedance bandwidth, and reflection coefficient [2].

To alleviate the shifting of operating frequencies in such scenarios, it is always better to design a wideband antenna. Taking into consideration above mentioned challenges, there is a dire demand for the design of a robust, compact, conformal, multiband/ wideband antenna for body-worn applications.

A CPW-fed octagonal shaped UWB antenna for WBAN application is reported in [3]. When the reported antenna is operated in close proximity to a human body, the radiation pattern of the antenna being bidirectional increased the specific absorption rate. To address this concern, authors in [3] have employed a full ground plane that is placed beneath the substrate layer to avoid the effect of radiations emitting from the antenna on the human body. A Bow-Tie antenna for biomedical applications is reported in [4]. When this antenna is placed over the skin, it operates in the frequency range of 0.5-2 GHz. However, the reported prototype is fabricated on a rigid PCB, which limits its application for the cases where conformality is required (on-body affixation).

In [5] and [6], authors have reported a biconical antenna for the body area network as it provides a directional pattern with minimum back radiation. The serious drawback of this antenna is its larger size which inhibits its usage in large-scale integration. Furthermore, in [7] the researchers reported that a big ground plane in an antenna shields the body from the electromagnetic (EM) radiation arising out of it by reducing the backward radiation. Nevertheless, antennas with large ground planes resulted in an increase in size and loss of flexibility in the wearable antenna. A pliable on-body antenna is presented in [8] which is compact, conformal, and has a unidirectional radiation pattern. The prospective antenna operates in the frequency band of 0.55-3 GHz when placed at different parts of the human body. In this antenna, the maximum SAR values remain well below 0.8 W/kg (10 g) for the maximum input power limited to 10 dBm. In [9], a unidirectional antenna meant for head imaging is reported. The dimensions of the prototype are $60 \times 85 \times 4$ mm^3 and work in the operational frequency range of 1.1-1.9 GHz. For the same application, an improved compact antenna is reported in [10] operating in the frequency band of 1- 4.3 GHz. A triple-band implantable antenna meant for biotelemetric application is proposed in [11], wherein the performance of the design is reported to have been achieved by utilizing the split ring resonators loaded with meandered lines in the radiating patch of the antenna. The fractional bandwidth achieved in all three operating bands of the antenna reported in [11] is less than 20% signifying the fact that the design is a narrow-band antenna. In [12], a flexible and compact circularly polarized monopole antenna is proposed for wearable applications. To achieve good performance in terms of gain and Specific Absorption Rate (SAR), the antenna is backed by an Artificial Magnetic Conductor (AMC) that acts as a reflector. A conformal wideband patch antenna backed by AMC for better SAR, impedance matching and high efficiency is reported in [31]. However, such types of designs as proposed in [12] and [31] have larger sizes and a higher degree of complexity. A low-profile Koch curve-inspired hybrid antenna is proposed in [13] for on-body WBAN applications. By virtue of fractal geometry with meandering slits and defected ground plane, the effective size has been miniaturized and bandwidth improvement has been achieved in the reported design [13].

In nutshell, it is observed that apart from the slot and traditional patches, versatile antenna designs for body worn applications with improved efficiency and performance have been recently reported [14], [36]. Keeping these challenges in mind, there is a dire need for new antennas that are more suitable for on-body operations.

The contribution of this paper can be summarized as:

- The fractal-based design used in this work ensures that the antenna is optimal in size by providing an increase in electrial length without an increase in area and offers dual-band of operation for interoperability covering WMTS (1395-1400, 1427-1432 MHz), ISM (2.4-2.484 GHz) and a portion of UWB bands [15], [35].
- A hybrid design is evolved by using the concept of fractals and rectangular loop; thereof the performance of the design is evaluated.
- The mathematical model of biological tissues and Moores curve are thoroughly discussed and are extended to this work.
- The bio-compatibility of the design is ensured by keeping the SAR well below the standard thresholds.

So, this work is a step toward mitigating the difficulties faced while designing the body-worn antennas for EM biomedical diagnostic systems.

Here FEM- based commercial software ANSYS HFSS v. 15.0 is utilized for designing and analyzing the prospective antenna. Furthermore, this writeup is divided into five sections; Section I provides a brief motivation about the work and insight into the latest designs proposed by the researchers, Section II discusses the geometrical layout of the proposed design and MTM properties of Moore's curve, Section III discusses the mathematical model of Moore's curve and biological tissues, results are analyzed and

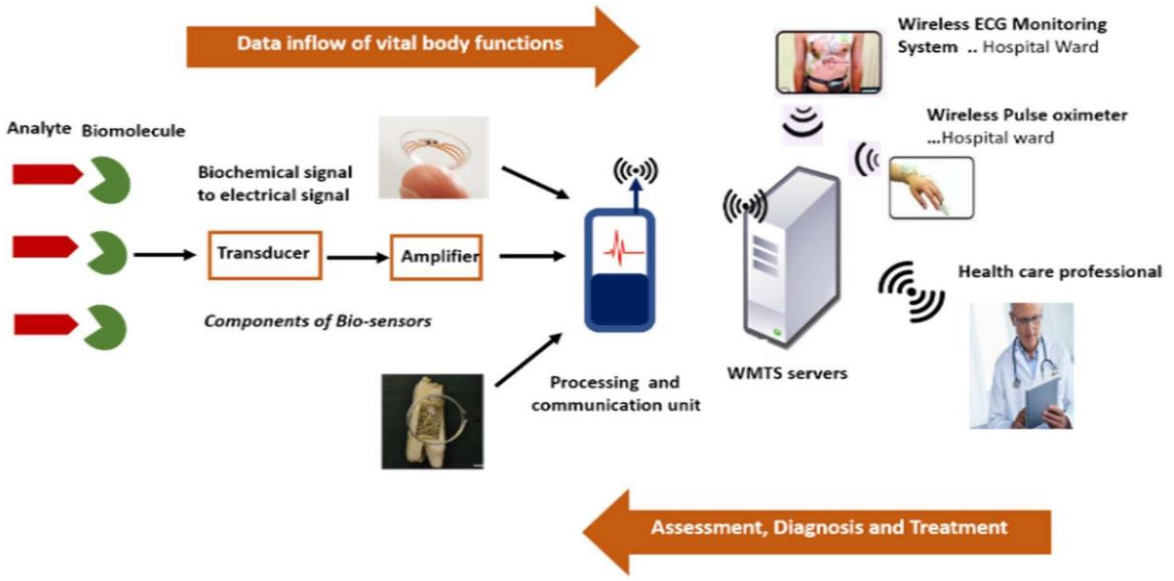

FIGURE 1. Bio-telemetry-based diagnostic system.

justified in Section IV, On-body performance(SAR analysis) in relation to bio-compatibility is evaluated in Section V, state of art comparison is carried out in Section VI and at last, the paper is concluded in Section VII.

II. PROPOSED DESIGN

A. GEOMETRICAL LAYOUT

This work is attributed to the development of an antenna for EM medical diagnostic systems and here forth we have chosen Moore's fractal-based antenna for this crucial application. The final design achieved in this work has undergone a number of evolutionary stages to achieve its optimal performance. Fig. 2 illustrates the schematic diagram of the proposed hybrid antenna fabricated on a 0.75 mm thick Rogers 5880 substrate with a loss tangent of 0.0009 and relative permittivity of 2.2. It is worth to mention that the Rogers RT/Duroid 5880 [16] is a high-frequency laminate made from a PTFE composite reinforced with glass microfibers. Furthermore, Rogers 5880 has an extremely low dielectric constant, low coefficient of thermal expansion, low dissipation factor and is remarkably resistant to corrosion, moisture and abrasion. Also, the Dielectric constant of the material remains constant over a wide frequency range. The glass-microfiber-reinforced PTFE laminate is ideal for single-bend applications. All these features make it an ideal material for forming, bending, broadband and high-frequency applications.

The prospective antenna consists of a top radiator that is evidently a hybrid version of the fractal-based Moore's antenna. The term hybrid used for the radiating element holds true in the context that the geometry of the antenna is a mixture of fractal concept and the conventional rectangular loop. To build the design, Moores curve of n= 4 is etched onto a rectangular patch succeeded by a rectangular loop within which it is enclosed. The fractal is excited through the rectangular loop (the fractal is connected to the loop through the patches at the diametrically opposite sides) that is connected to the feedline. Furthermore, the ground of the proposed antenna is partial and the three slots are embedded within it for achieving impedance matching and suppressing the back lobe radiation. For the size reduction of the antenna, we employed Moore's fractal geometry which in turn lowered the operating frequency of the antenna by increasing its electrical length that results in achieving the required compactness [13].

TABLE 1. Parameters of the geometrical layout of proposed design.

Parameter	Value (mm)	Parameter	Value (mm)
L	19.5	W_g	6.5
W	17	L_g	20
R	8	S1	5
W_f	2.51	S2	2.2
L_f	8.83	W_s	1
Lsc	9	Lse	18

It is a well established fact that the dimensions of the ground if modified can change the antenna impedance and therefore can help in selecting the desired band of operation [17]. The overall planar size of the prototype is $0.135\lambda_0 \times 0.093\lambda_0$ where λ_0 is the wavelength of the lowest resonating frequency. The radiating element is fed by a rectangular feedline of length L_f and width W_f. All the optimized parameters of the geometrical layout are tabulated in Table 1. The width, length, and position of the slots etched in the ground have been optimized for achieving better performance.

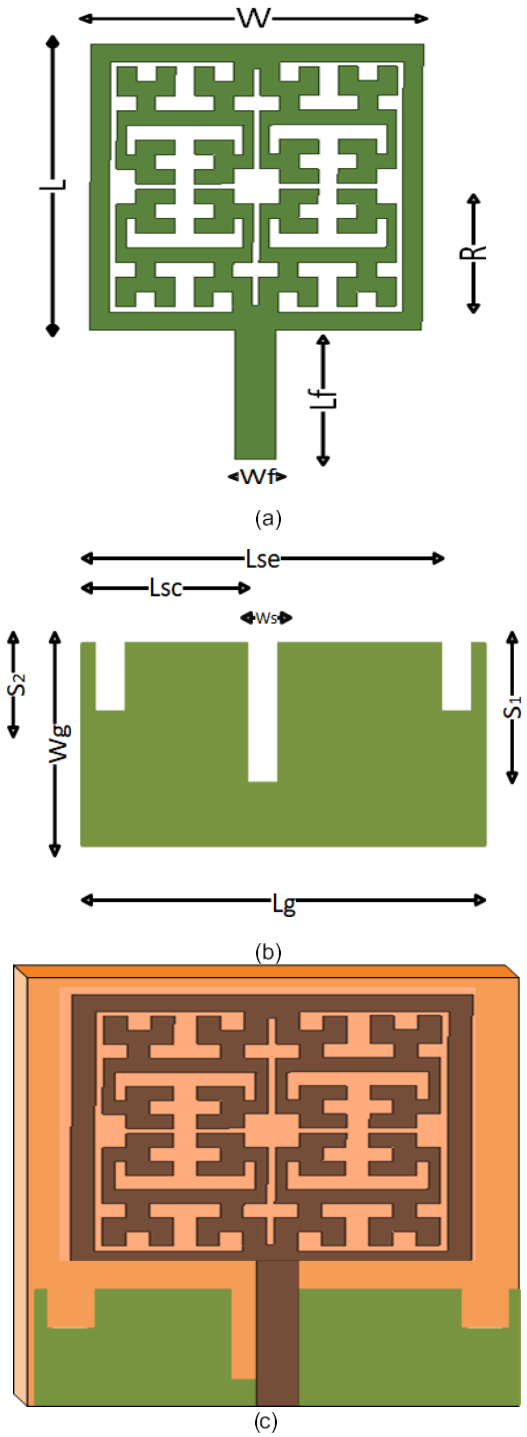

FIGURE 2. Geometrical layout of the antenna a) top view b) bottom view c) perspective view.

B. METAMATERIAL PROPERTIES(MTM)

The Moore curve being a variant of Hilbert curve with the feature of end points connected belongs to the class of continuous fractal space-filling curve. The MTM behavior of Hilbert curve has been reported extensively in [18], [19], and [20] recently. The EM behavior of the hybrid fractal reported in this article is discussed in light of the simulations carried out. To demonstrate the MTM property of a Moore curve, an M_3 curve is modeled as PEC on a Rogers/RT Duroid 5880 substrate with permittivity of 2.2, and a loss tangent of 0.0009. In a two-port system, the M_3 curve modeled is put under test (located between two waveguide ports) with orthogonal electric and magnetic boundary conditions.

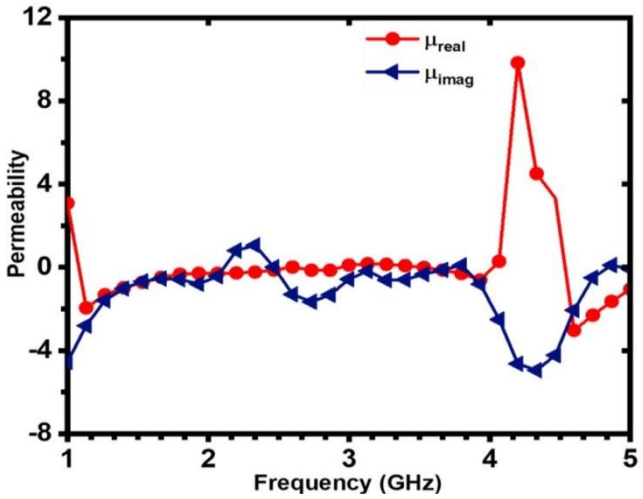

FIGURE 3. Complex effective permeability of M3 curve.

Fig. 3 shows the extracted real and imaginary parts of the effective permeability based on the calculated S-parameters [21], [33]. In Fig. 3(b), negative permeability is observed in the frequency range of 1.25-2 GHz and 2.4-4.4 GHz. It demonstrates the metamaterial behavior of a Moore curve resonator.

In order to understand operation of the proposed antenna in two different case scenarios (on-body and free space), the mathematical modeling of the human tissue and the proposed design is discussed in detail in next section.

III. MATHEMATICAL MODELLING

A. BIOLOGICAL TISSUES

In this section, a mathematical model of the tissues is discussed thoroughly as our work involves the human body. A lot of effort has been put in by researchers to model the tissues by studying the dielectric properties of biological tissues. The frequency-dependent electrical properties of the tissues were lately discussed by Schwan and Foster in 1957. It is a well-known fact that above 100 Hz, the relative permittivity decreases in a three phased staged manner; in α, β and γ dispersion regions. The well-known Debye equation (Equation1), a first order approximation of the complex permittivity ε as a function of the angular frequency ω can be used to mathematically define the dielectric property of tissues in these regions [22].

$$\varepsilon(\omega) = \varepsilon_{\infty} + \frac{\varepsilon_s - \varepsilon_{\infty}}{1 + j\omega\tau} \quad (1)$$

The intensity of the dispersion is given by $\Delta\varepsilon = \varepsilon_s - \varepsilon_{\infty}$, where ε_{∞} denotes the permittivity at $\omega\tau$ 1, ε_s the permittivity at $\omega\tau$ 1 and $\tau\tau$ as the time constant assigned to each

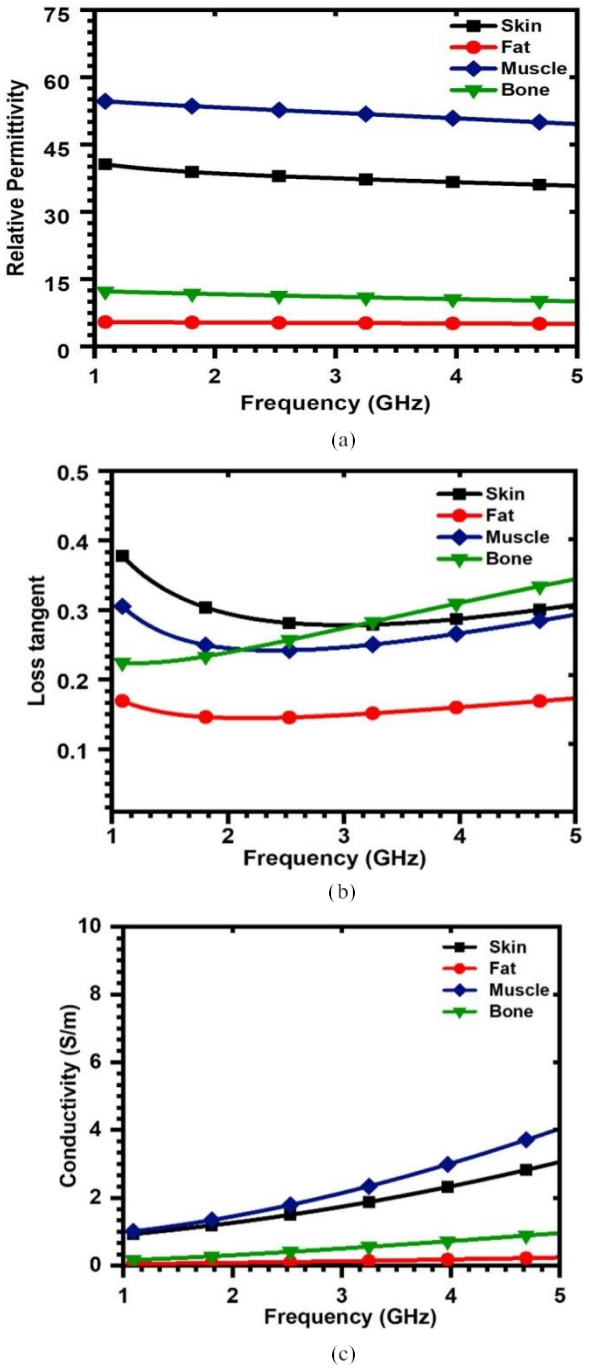

FIGURE 4. Frequency-dependent plots of human tissue a) Relative permittivity b) Loss tangent c) Conductivity.

of these relaxation regions. To extend this equation to other dispersion regions, a distribution parameter α is introduced in the above equation. The distribution parameter describes the bandwidth of the related relaxation region and thereof the Debye equation is extended to the Cole-Cole equation in the manner of

$$\varepsilon(\omega) = \varepsilon_\infty + \frac{\Delta\varepsilon}{1 + (j\omega\tau)^{1-\alpha}} \tag{2}$$

In order to extend this equation to all of the three regions, summation from n = 1 to 4 is introduced in the equation. To cover the static conductivity of body tissues an additional term, σ_i is introduced in the equation.

$$\varepsilon(\omega) = \varepsilon_\infty + \sum_{n=1}^{4} \frac{\Delta\varepsilon_n}{1 + (j\omega\tau_n)^{1-\alpha_n}} + \frac{\sigma_i}{j\omega\varepsilon_o} \tag{3}$$

The constants $\Delta\varepsilon_n$, τ_n, α_n with n = {1, 2, 3, 4}, ε_∞, and σ_i are Gabriel parameters. On taking into account all these parameters, the mathematical model of the multilayer tissue model for this work is developed.

The frequency dependent plots of electrical properties of human tissues (skin, fat muscle and bone) are illustrated in Figure 4.

The important parameter for an antenna utilized for biotelemetric application is the amount of power absorbed by the human body or in specific terms Specific absorption rate (SAR). Researchers, academicians and engineers have a concern about the health impact of radiation and therefore it is important to keep a check on it for determining the biocompatibility of the device. SAR is defined as the rate at which the body absorbs EM power per unit mass and is expressed by Equation 4 [23], [24].

$$\text{SAR} = \frac{1}{V} \int \frac{\sigma(r)|E(r)|^2}{\rho(r)} dr \tag{4}$$

where σ , ρ and V represent conductivity, mass density and volume of the sample tissue, respectively and E is the rms electric field. The average value (over 10 g) of SAR should not exceed 2 W/Kg as per the IEEE C95.1- 2005 standard [24].

B. MOORES CURVE

This section deals with principles behind the Moore curve. It is a well-established fact that Moore's fractal curve as well as the Hilbert curve belongs to the group of space-filling types. Over and above, it needs to be mentioned that the Moore curve is a variant of the Hilbert curve with its ends connected. In this case of Moore's inspired antenna, the length of each Moore segment with a side dimension L and order n, d_n is expressed in equation 1. Fig. 5 demonstrates Moore's curve for the first four iterations. After studying the two curves, it is observed that the perimeter of a closed Moore pre-fractal is equal to the total number of line segments of Hilbert curve plus one. Furthermore, the perimeter for the Hilbert space-filling curve is given by $S_{n,H}$ [25]. Also, the length of the line segment of the curve is given by d_n

$$d_n = \frac{L}{2^n - 1} \tag{5}$$

$$S_{n,H} = 2^n + 1 \; L \tag{6}$$

On extending the Equation 6 to the Moore space-filling curve of the same order, n, the total perimeter will be

$$S_{n,M} = 2^n + 1 + \frac{1}{2^n - 1} L \tag{7}$$

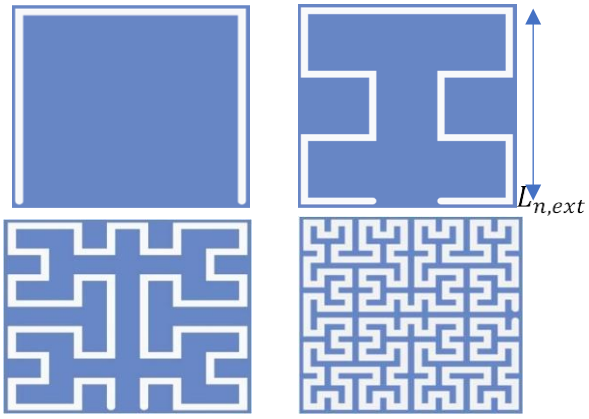

FIGURE 5. The Ist, the 2nd, the 3rd and the 4th iteration for Moore fractal curves.

Extending these equations to the current work, the perimeter of the rectangular loop is also included. Therefore, the total perimeter of the radiating element is

$$S \quad 2^n \quad 1 \quad \frac{1}{2^n - 1} L = + 2 (L_{r1} + W_{r1}) + 2 (L_{r2} + W_{r2}) \tag{8}$$

The external side length of the slot, $L_{n,ext}$ at any iteration n, taking into account the slot width *w* and the spacing between slots *g*, can be expressed as [26]

$$L_{n,ext} = 2^n (w + g) - g \tag{9}$$

The lowest resonant frequency, f_{01} of the structure relative to the perimeter is formulated by [27]

$$f_{01} = \frac{c}{2L_{n,ext}\sqrt{\varepsilon_{eff}}} \tag{10}$$

IV. RESULTS AND DISCUSSION

A. DESIGN EVOLUTION OF PROSPECTIVE ANTENNA AND PARAMETRIC ANALYSIS

The prospective antenna offering dual-band performance was developed in four main stages. First, the dimensions of the design were calculated in free space wavelength at the lowest operating frequency (1.4 GHz). Then, the current path was increased by introducing the fractal structure on the radiator resulting in the compactness of the design and shifting of resonant frequency towards lower values. Fig. 6 illustrates the response of the design on the phantom with radiating patch consisting of only Moore's fractal curve. It is quite evident from the simulated results that the prospective antenna at this evolution stage is a single band antenna with a wideband resonance ranging from 2.2 to 4.2 GHz. It is apparent from the simulated results that the rectangular loop along with the open-ended slots placed on the ground plane affects the lower band, the upper band is more influenced by the current flow in the fractal curve of the radiating patch.

In the next step, the fractal structure was enclosed in a rectangular loop resulting in the creeping in of an additional

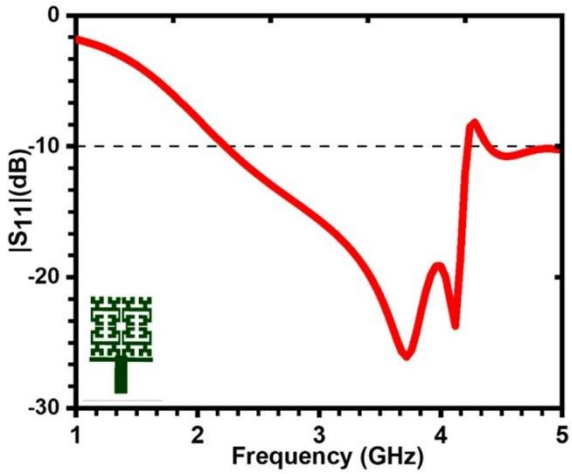

FIGURE 6. Reflection coefficient of prospective design with simple Moore's fractal radiating patch.

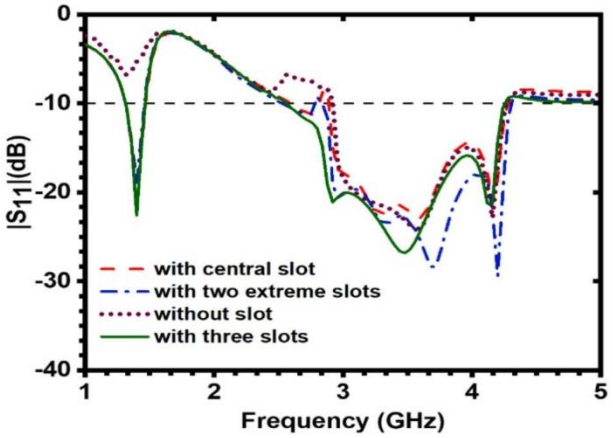

FIGURE 7. Effect of slots on the return loss characteristics of the design.

(small) resonance at 1.32 GHz. Fig. 7 shows the return loss of the antenna with and without the slots in the ground plane.

On using an open-ended central slot in the ground, the impedance bandwidth of the antenna gets enhanced. With the incorporation of two extreme symmetric open-ended slots in the ground in the final stage, the impedance matching of the design improved in both of the bands and the resonant frequency in the upper band is shifted towards a lower value. As observed in Fig. 7, incorporation of slots in the ground plane helps in achieving dual-band characteristics.

B. EXPERIMENTAL VERIFICATION OF THE PROSPECTIVE DESIGN

The proposed antenna was fabricated and then the return loss and radiation pattern measurements of the prototype were performed at the University of Kashmir, SPACE laboratory. Fig. 8a illustrates the simulated and measured return loss of the Hybrid antenna in free space. It is evident that the prototype exhibits dual-band operation with center frequencies at 1.4 GHz & 3.58 GHz in free space.

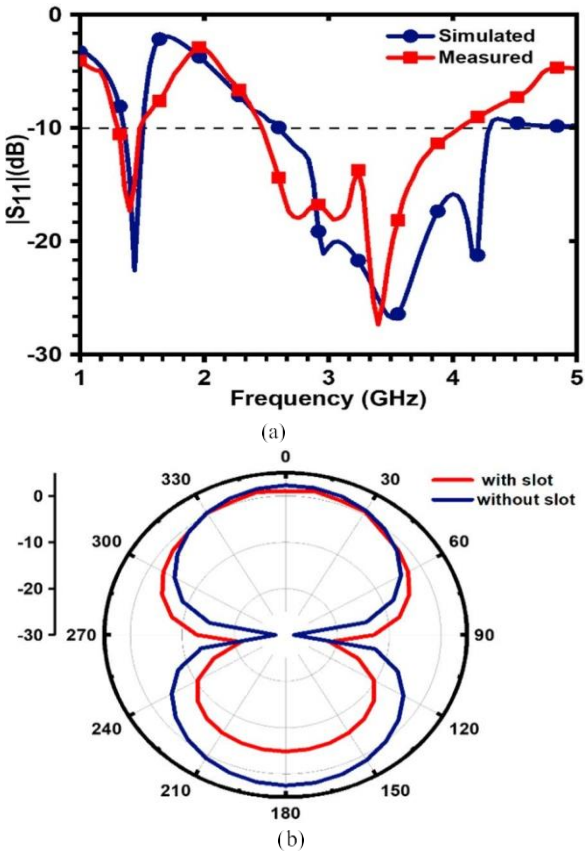

FIGURE 8. a) Reflection coefficient vs frequency of antenna in free space b) Gain of the design with and without slots incorporated in free space for $\varnothing = 0^\circ$.

The corresponding impedance bandwidth of 170 MHz (1.3-1.47 GHz) and 1750 MHz (2.5-4.25 Hz) is achieved respectively. However, there is a slight shift in the upper-frequency band towards lower values in the measured return loss characteristics as is evident in Fig. 8a. On rigorously analyzing the frequency of operation, the lowest resonant frequency of the hybrid design can be approximated by Equation 11 where s_s is the perimeter of the design.

$$f_{01} = \frac{c}{s_s \sqrt{\varepsilon_{eff}}} \tag{11}$$

The effect of slots incorporated in the ground plane of design (in free space) on the radiation pattern is analyzed in Fig. 8b. It is observed that the incorporation of slots results in the reduction of the back lobe that is likely to interact with the human tissue. The directional radiation of antenna is improved in the final design of the proposed antenna.

For validating the simulated results, the performance of the antenna is measured using Keysight *N5247A Microwave Network Analyzer*. In real scenario, the antenna is placed at two different positions on the body for measuring its performance (Fig. 9). The idea behind placing of the antenna at different positions is to determine its robustness to bending and also to evaluate the effect of variation in electrical properties of different parts of the body on the performance of antenna.

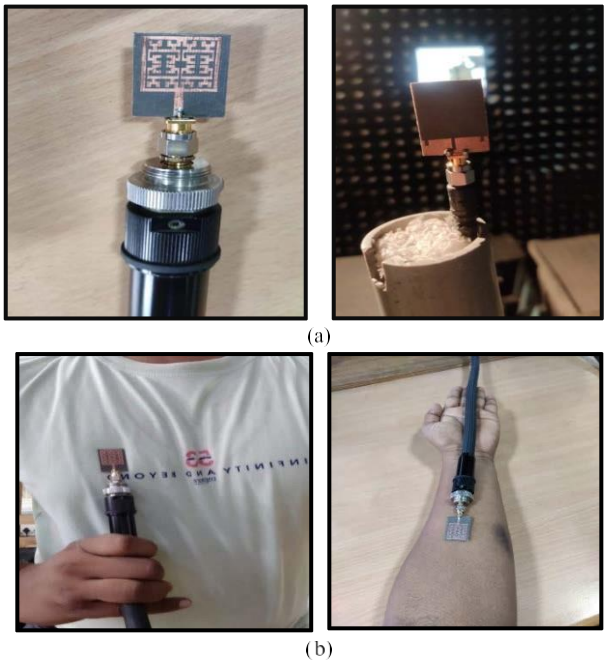

FIGURE 9. Antenna under measurement a) in anechoic chamber b) Placement of antenna over different parts of the body.

Fig. 9 b illustrates how the antenna has been placed on a human arm and chest for evaluating its efficacy.

Furthermore, Fig. 10 demonstrates the measured and simulated variation of the reflection coefficient over a frequency range of 1-5GHz when the antenna is placed at different positions (chest and arm) on the human body. Measured and simulated return loss shows good agreement in terms of return loss characteristics and bandwidth. The measured bandwidth of the antenna, when placed on the arm, is approximately 420 MHz (1.38-1.8 GHz)/ 2630 MHz (2.25-4.88) whereas the simulated bandwidth of the design for the same configuration is 420 MHz (1.42-1.84 GHz) /2440 MHz (2.42-4.86 GHz). In the second scenario when the prototype is placed on the chest, the measured bandwidth of the design is approximately 400MHz (1.30-1.70 GHz) / 2420 MHz (2.38-4.7) and the simulated bandwidth is 160 MHz (1.3-1.46 GHz) /2360 MHz (2.50-4.86 GHz). When the prototype is placed over the arm (cylindrical model), there is a slight change in the reflection coefficient i.e., the frequency range of the second resonating band gets slightly shifted towards the lower frequencies owing to the detuning effect of the human body.

One of the parameters utilized in this work for comparing the performance of our design with the other reported designs is Fractional Bandwidth (FBW). It can be calculated using Equation 12.

$$\text{FBW} = \frac{f_h - f_l}{f_h + f_l} \times 200\% \tag{12}$$

The value of FBW varies between 0 and 200%. Antennas with FBW greater than 20% are referred to as wideband antennas and those with greater than 50% are ultra-wideband antennas respectively.

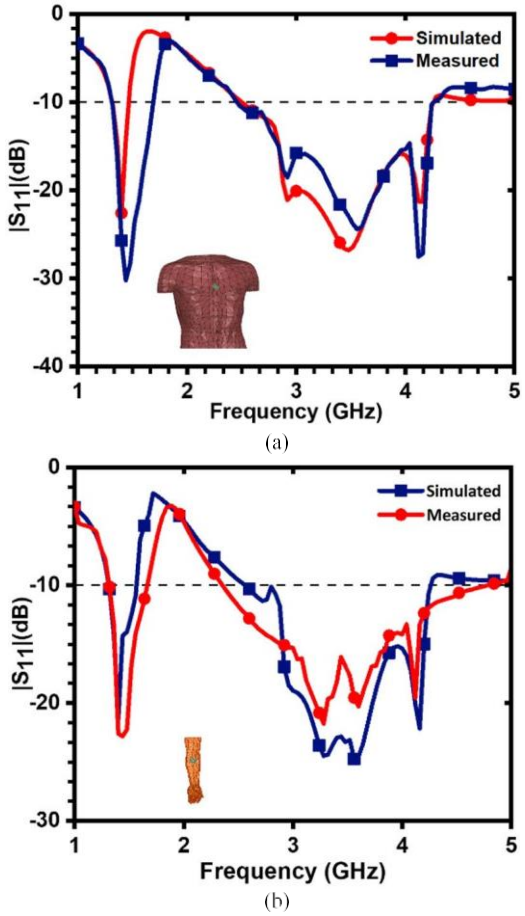

FIGURE 10. Simulated and measured reflection coefficient of the antenna when placed on a) chest b) arm.

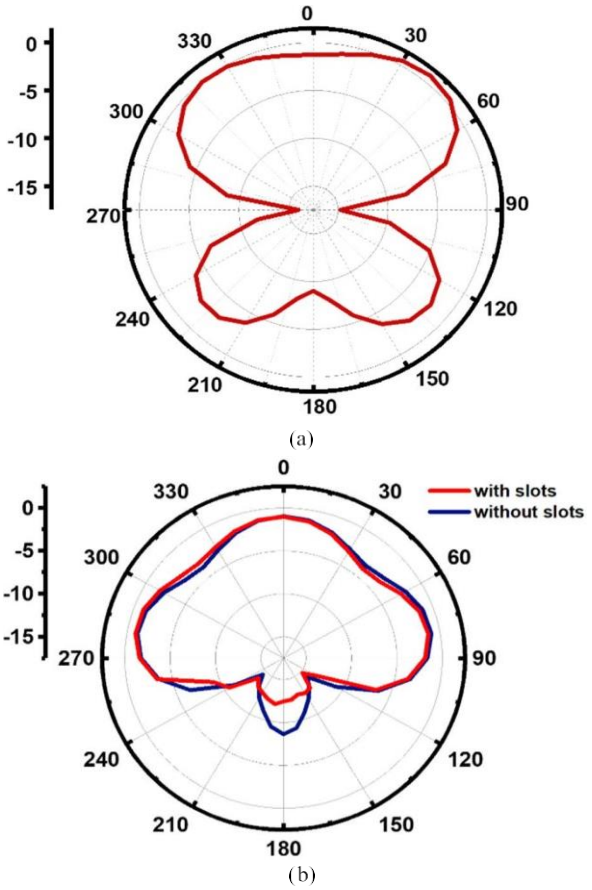

FIGURE 11. Simulated radiation Pattern of the design at a) $\varnothing = 0^\circ$ b) $\varnothing = 90^\circ$ on placing the antenna on a phantom.

On comparing the simulated and the measured results, the simulated bandwidth is less than the measured bandwidth; this difference is attributed to small geometrical inaccuracies that occur during fabrication and measurement assembly. The antenna covers the bands meant exclusively for bio-telemetry; ISM/WMTS/UWB/Wireless Personal Communication. The designed antenna is validated for both the free space and on-body operating conditions.

The 2D radiation pattern as shown in Fig. 8b and 11 endorses the observation that there is a significant reduction in gain value from 2.5 dBi in free space to 1.1 dBi when placed over the phantom. Due to the stark disparity between the dielectric properties of human tissues and air, the process of absorption and reflection is responsible for the significant decrease in the value of gain. Since the back lobe of the radiation pattern of the antenna has already been reduced in the design by incorporating the central slot as illustrated in Fig. 6b, therefore the prototype maintains a low-key interaction with the body in comparison to the design without a slot.

In addition to this, on analyzing the surface distribution current in Fig. 11, it is observed that the stronger surface currents are concentrated towards the center of the vertical slot which is directed oppositely on either side of the slots in the ground. The oppositely directed current with equal amplitude on either side of the central slot leads to a transmission line mode; thereby the E & H fields in the perpendicular direction get canceled out and hence the back lobes are minimized. This technique of etching the slots in the ground has also been utilized in [28] and [37].

In nutshell, it is observed that the reduced reflected currents in the prototype lead to the reduction of back lobe radiations to below -7 dB. Also, the 3D radiation pattern of the prospective design on the human body is illustrated in Fig. 13. To analyze and clearly understand the bio-compatibility of the reported antenna, its on-body performance is realized in the next section.

V. ON-BODY PERFORMANCE

The effects of high conductivity and permittivity of human tissues on the performance of the antenna is thoroughly studied in this section.

In body-worn antennas, EM waves interact with the body and therefore, it becomes imperative to understand the biological and thermal aspects in such situations. A multi-layer tissue has been utilized in the simulating environment for understanding the behavior of the prospective antenna in comparison to an average body model. The reason for utilizing the multilayer model is that it provides a clear picture

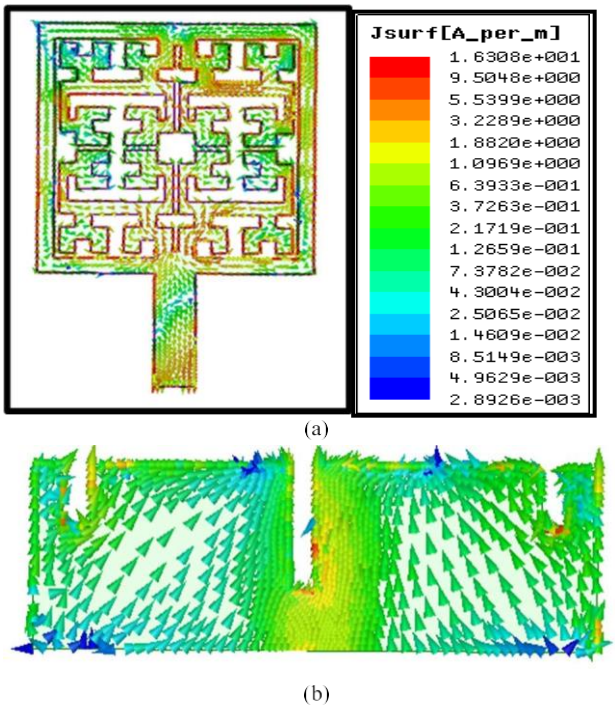

FIGURE 12. Surface current distribution in a) radiating patch element b) ground.

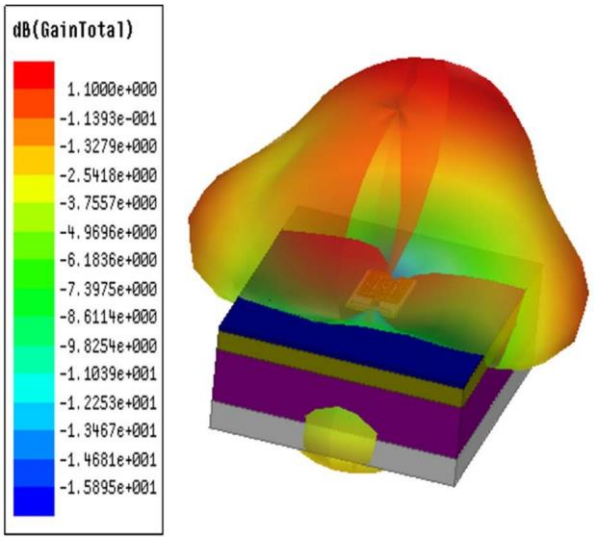

FIGURE 13. 3D radiation pattern of the prospective antenna.

of the effect of a human body on the performance of the antenna than an average body model (single tissue model). For numerical simulation of the antenna, a multilayer human tissue (100 mm $\times$100 mm $\times$45 mm) is modeled as illustrated in Fig. 13. The dielectric characteristics of a modeled multi-layer tissue at 2.45 GHz in the present work are tabulated in Table 2. Fig. 13 gives us clear insight into the manner in which the antenna is placed over the phantom. The multilayer tissue modeled in this work consists of skin, fat, muscle, and bone tissues with thicknesses of 2mm, 8mm, 23mm and 12mm respectively.

TABLE 2. Dielectric characteristics of human tissues [30].

Tissue	Thick-ness (mm)	Permittivity	Conductivity (S/m)	Loss Tangent	Density (kg/m^3)
Skin	2	31.29	8.013	0.2835	1100
Fat	8	4.602	0.585	0.1938	1100
Muscle	23	52.79	1.705	0.2419	1060
Bone	12	12.66	3.859	0.252	1850

TABLE 3. Main performance parameters of the designed antenna.

Bandwidth (GHz)	Condition	Efficiency	SAR (W/Kg)	Gain (dB)
1.38-1.8	Sim. In Free Space	$\approx$0.957	-	2.2
	Meas. in Free space	-	-	1.9
	Sim. On body	$\approx$0.750	0.025	0.91
	Meas. On body	-	-	-
2.2 – 4.8	Sim. In Free Space	$\approx$0.912	-	2.31
	Meas. in Free space	-	-	1.85
	Sim. On body	$\approx$0.652	0.18	0.98-1.1
	Meas. On body	-	-	-

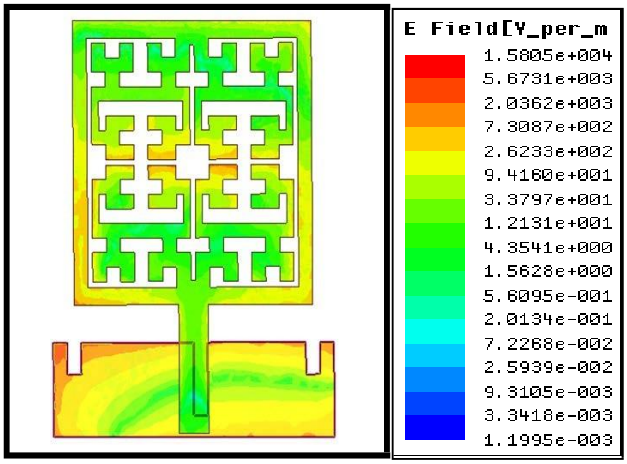

FIGURE 14. Electrical field distribution over the antenna.

In order to understand the incidence of hot spots on the body beneath the antenna, the distribution of the electric field is analyzed at the resonant frequencies. It is observed from Fig. 14 that the magnitude of the electric field is higher at the edges of the ground and the slots incorporated in it. In cor-respondence to this, hot spots are observed on the skin at these points. Furthermore, the hot spot is also found where the maximum electric field is observed on the top radiating element.

The radiation pattern of the prospective antenna provides insight into the SAR distribution. It is observed that the antenna radiates maximum energy away from the prototype

VI. PERFORMANCE COMPARISON

On comparing our prototype with the recently reported ones, it is observed that the average SAR is very less than the other designs for the maximum input power. Furthermore, it is evi- dent from Table 4 that the antenna is semi-flexible as reported in [12], [33], and [34], wideband (in both of the bands) with a reduced back lobe and above all offers a dual-band of oper-ation making it a better choice for interoperability. While studying antennas for biotelemetric/diagnostic systems, it is to be noted that lower SAR seems to be of significance when the power input to the design is sufficient enough for the optimal working of the system. So, in the reported works, the value of input power is noted for comparison of the efficacy of the system. Designs reported in [8] and [9] have minimal size, offer a wideband frequency range but are single band limiting their interoperability usage, and have a higher magnitude of SAR for a lower value of input power in comparison to this work. Even though the design reported in [29] has a miniature size, offers less SAR, and offers a triple band but it suffers due to its narrowband characteristics making it susceptible to frequency detuning due to body postures and movements. Here forth, it can be concluded that the performance of the proposed prototype is far better than the others making it an ideal candidate for wearable applications.

VII. CONCLUSION AND FUTURE WORK

A compact, robust and flexible body-worn antenna is pro- posed for biotelemetry in biomedical diagnostic systems. The fractal-based design increased the length of current flow thereby ensuring that the antenna is of optimal size and is operating at a lower frequency of interest. The antenna offers dual-band operation (1.38-1.8 GHz and 2.25-4.88 GHz) cov-ering WMTS and ISM bands simultaneously; making it an ideal candidate for interoperability in biomedical applica- tions. The hybrid antenna reported in this paper offers a fractional bandwidth of about 38.5% and 73.7% in the dual

bands 1.38-1.8 GHz and 2.25-4.88 GHz respectively. The back lobe has been minimized to some extent in this work by inserting the vertical slots in the ground. The peak gain of
2.2 dBi has been achieved in the free space and 1.1 dBi when the proposed design is placed on the phantom. The specific absorption rate is well below 0.025 W/kg for an input power of 24 dBm≈ which is generally used for SAR measurement in the case of mobile application devices. The prospective antenna has an edge over the recently proposed antennas due to its compact size, interoperability, and above all its low specific absorption rate for high power input. Mathematical models of entities involved in this work are also discussed to provide insight into the designing of the radiating element of the antenna and phantom respectively. To validate the simu- lated results, the device was fabricated and its performance was evaluated using Keysight N5247A Microwave Network Analyzer. To the best of our knowledge, the proposed design is the most compact antenna that offers the lowest SAR for maximum power input and dual-band covering most of the bands allocated for biotelemetry. This work can be extended to investigate the device for imaging applications. Also, the device (because of its minimized size) can be employed in an array configuration for further improvement of gain.

REFERENCES

[1] S. Movassaghi, M. Abolhasan, J. Lipman, D. Smith, and A. Jamalipour, ''Wireless body area networks: A survey,'' *IEEE Commun. Surveys Tuts.*, vol. 16, no. 3, pp. 1658–1686, 3rd Quart., 2014.

[2] M. N. Shakib, M. Moghavvemi, and W. N. L. B. W. Mahadi, ''Design of a tri-band off-body antenna for WBAN communication,'' *IEEE Antennas Wireless Propag. Lett.*, vol. 16, pp. 210–213, 2017.

[3] L. A. Y. Poffelie, P. J. Soh, S. Yan, and G. A. E. Vandenbosch, ''A high-fidelity all-textile UWB antenna with low back radiation for off-body WBAN applications,'' *IEEE Trans. Antennas Propag.*, vol. 64, no. 2, pp. 757–760, Feb. 2016.

[4] X. Li, M. Jalilvand, Y. L. Sit, and T. Zwick, ''A compact double-layer on-body matched bowtie antenna for medical diagnosis,'' *IEEE Trans. Antennas Propag.*, vol. 62, no. 4, pp. 1808–1816, Apr. 2014.

[5] M. Klemm, I. Z. Kovcs, G. F. Pedersen, and G. Troster, ''Novel small-size directional antenna for UWB WBAN/WPAN applications,'' *IEEE Trans. Antennas Propag.*, vol. 53, no. 12, pp. 3884–3896, Dec. 2005.

[6] N. Chahat, M. Zhadobov, R. Sauleau, and K. Ito, ''A compact UWB antenna for on-body application,'' *IEEE Trans. Antennas Propag.*, vol. 59, no. 4, pp. 1123–1131, Apr. 2011.

[7] A. Y. I. Ashyap, S. H. B. Dahlan, Z. Z. Abidin, M. I. Abbasi, M. R. Kamarudin, H. A. Majid, M. H. Dahri, M. H. Jamaluddin, and A. Alomainy, ''An overview of electromagnetic band-gap integrated wearable antennas,'' *IEEE Access*, vol. 8, pp. 7641–7658, 2020.

[8] A. S. M. Alqadami, N. Nguyen-Trong, A. E. Stancombe, K. Bialkowski, and A. Abbosh, ''Compact flexible wideband antenna for on-body electromagnetic medical diagnostic systems,'' *IEEE Trans. Antennas Propag.*, vol. 68, no. 12, pp. 8180–8185, Dec. 2020.

[9] A. S. M. Alqadami, K. S. Bialkowski, A. T. Mobashsher, and A. M. Abbosh, ''Wearable electromagnetic head imaging system using flexible wideband antenna array based on polymer technology for brain stroke diagnosis,'' *IEEE Trans. Biomed. Circuits Syst.*, vol. 13, no. 1, pp. 124–134, Feb. 2019.

[10] A. S. M. Alqadami, N. Nguyen-Trong, B. Mohammed, A. E. Stancombe, M. T. Heitzmann, and A. Abbosh, ''Compact unidirectional conformal antenna based on flexible high-permittivity custom-made substrate for wearable wideband electromagnetic head imaging system,'' *IEEE Trans. Antennas Propag.*, vol. 68, no. 1, pp. 183–194, Jan. 2020.

[11] Y. E. Yamac, M. Ciflik, and S. C. Basaran, ''Miniaturized multiband implantable antenna designs for in-body compact medical devices,'' *Int. J. RF Microw. Comput.-Aided Eng.*, vol. 32, no. 11, Jul. 2022, Art. no. e23335.

[12] Y. B. Chaouche, M. Nedil, I. B. Mabrouk, and O. M. Ramahi, ''A wearable circularly polarized antenna backed by AMC reflector for WBAN communications,'' *IEEE Access*, vol. 10, pp. 12838–12852, 2022, doi: 10.1109/ACCESS.2022.3146386.

[13] A. Arif, M. Zubair, M. Ali, M. U. Khan, and M. Q. Mehmood, ''A compact, low-profile fractal antenna for wearable on-body WBAN applications,'' *IEEE Antennas Wireless Propag. Lett.*, vol. 18, no. 5, pp. 981–985,May 2019, doi: 10.1109/LAWP.2019.2906829.

[14] A. Y. I. Ashyap, Z. Z. Abidin, S. H. Dahlan, H. A. Majid, M. R. Kamarudin, A. Alomainy, R. A. Abd-Alhameed, J. S. Kosha, and J. M. Noras, ''Highly efficient wearable CPW antenna enabled by EBG-FSS struc-ture for medical body area network applications,'' *IEEE Access*, vol. 6,pp. 77529–77541, 2018.

[15] J. Anguera, A. Andújar, J. Jayasinghe, V. V. S. S. S. Chakravarthy, P. S. R. Chowdary, J. L. Pijoan, T. Ali, and C. Cattani, ''Fractal antennas: An historical perspective,'' *Fractal Fractional*, vol. 4, no. 1, p. 3, Jan. 2020.

[16] *RT/Duroid 5870/5880 High Frequency Laminates*, Rogers Corp., Chandler, AZ, USA, Rogers 5880, 2022.

[17] A. T. Abed, M. S. J. Singh, V. Thiruchelvam, S. Duraikannan, O. A. Tawfeeq, B. A. Tawfeeq, and M. T. Islam, ''Challenges and limits of fractal and slot antennas for WLAN, LTE, ISM, and 5G communication: A review paper,'' *Ann. Telecommun.*, vol. 76, nos. 9–10, pp. 547–557, Oct. 2021.

[18] E. Motovilova and S. Y. Huang, ''Hilbert curve-based metasurface to enhance sensitivity of radio frequency coils for 7-T MRI,'' *IEEE Trans. Microw. Theory Techn.*, vol. 67, no. 2, pp. 615–625, Feb. 2019, doi: 10.1109/TMTT.2018.2882486.

[19] W. J. Krzysztofik, ''Fractals in antennas and metamaterials applications,'' in *Fractal Analysis: Applications in Physics, Engineering and Technology*. London, U.K.: IntechOpen, 2017.

[20] T. A. Elwi, Z. A. A. Hassain, and O. A. Tawfeeq, ''Hilbert metamaterial printed antenna based on organic substrates for energy harvesting,'' *IET Microw., Antennas Propag.*, vol. 13, no. 12, pp. 2185–2192, Oct. 2019.

[21] X. Chen, T. M. Grzegorczyk, B.-I. Wu, J. Pacheco, Jr., and J. A. Kong, ''Robust method to retrieve the constitutive effective parameters of metamaterials,'' *Phys. Rev. E, Stat. Phys. Plasmas Fluids Relat. Interdiscip. Top.*, vol. 70, no. 1, 2004, Art. no. 016608.

[22] H. S. Hershkovich, N. Urman, O. Yesharim, A. Naveh, and Z. Bomzon, ''The dielectric properties of skin and their influence on the delivery of tumor treating fields to the torso: A study combining in vivo measurements with numerical simulations,'' *Phys. Med. Biol.*, vol. 64, no. 18, Sep. 2019, Art. no. 185014.

[23] H. R. Raa, A. I. Abbosh, H. M. Al-Rizzo, and D. G. Rucker, ''Flexible and compact AMC based antenna for telemedicine applications,'' *IEEE Trans. Antennas Propag.*, vol. 61, no. 2, pp. 524–531, Feb. 2013.

[24] *IEEE Recommended Practice for Measurements and Computations of Radio Frequency Electromagnetic Fields With Respect to Human Exposure to Such Fields, 100 kHz–300 GHz*, IEEE Standard C95.3-2002 (Revision of IEEE Standard C95.3-1991), 2002, pp. 1–126.

[25] R. Yee and L. Liu, ''An iterated function system based method to generate Hilbert-type space-filling curves,'' *Int. J. Inf. Technol. Comput. Sci.*, vol. 7, no. 12, pp. 12–22, Nov. 2015.

[26] M. Barra, C. Collado, J. Mateu, and J. M. O'Callaghan, ''Miniaturization of superconducting filters using Hilbert fractal curves,'' *IEEE Trans. Appl. Supercond.*, vol. 15, no. 3, pp. 3841–3846, Sep. 2005.

[27] J. K. Ali, ''A new microstrip-fed printed slot antenna based on Moore space-filling geometry,'' in *Proc. Loughborough Antennas Propag. Conf.*, Nov. 2009, pp. 449–452.

[28] W.-G. Lim, H.-S. Jang, and J.-W. Yu, ''New method for back lobe suppression of microstrip patch antenna for GPS,'' in *Proc. 40th Eur. Microw. Conf.*, Paris, France, Sep. 2010, pp. 679–682.

[29] A. Gupta and V. Kumar, ''Design of a tri-band patch antenna with back reflector for off-body communication,'' *Wireless Pers. Commun.*, vol. 115, no. 1, pp. 173–185, Nov. 2020.

[30] Y. Fan, X. Liu, J. Li, and T. Chang, ''A miniaturized circularly-polarized antenna for in-body wireless communications,'' *Micromachines*, vol. 10, no. 1, p. 70, Jan. 2019.

[31] A. Gupta, A. Kansal, and P. Chawla, ''Design of a wideband patch antenna and performance enhancement using an AMC reflector surface for on-body communication at 2.45 GHz,'' *Int. J. Electron.*, pp. 1–16, May 2022.

[32] S. Bhattacharjee, M. Mitra, and S. R. B. Chaudhuri, ''An effective SAR reduction technique of a compact meander line antenna for wearable applications,'' *Prog. Electromagn. Res. M*, vol. 55, pp. 143–152, 2017